ChemPubSoc Europe

DOI: 10.1002/cphc.201900564

CHEMPHYSCHEM Articles

Special Issue

Correlating Oxygen Reduction Reaction Activity and Structural Rearrangements in MgO-Supported Platinum Nanoparticles

Kevin Rossi,[a, b] Gian Giacomo Asara,[a] and Francesca Baletto*[a]

We develop a multi-scale approach towards the design of metallic nanoparticles with applications as catalysts in electrochemical reactions. The here discussed method exploits the relationship between nanoparticle architecture and electrochemical activity and is applied to study the catalytic properties of MgO(100)-supported Pt nanosystems undergoing solid-solid and solid-liquid transitions. We observe that a major increment in the activity is associated to the reconstruction of the interface layers, supporting the need for a full geometrical characterisation of such structures also when in-operando.

1. Introduction

Green electrochemistry technologies play a fundamental role in reversing environmental pollution.[1] Among these, fuel cells are attracting considerable attention as substitutes of carbon-based fuel engines. Their large-scale commercialisation is however currently hindered by the sluggishness of the electrochemical reduction of oxygen (ORR) catalysed at the cathode.[2] Delivering robust and practical guidelines in predicting, controlling, and designing candidates for optimising acatalytic reaction – e.g. oxygen reduction reaction in fuel cells – can dramatically decrease the cost and/or the environmental impact of any chemical process. The mechanistic understanding of chemical reaction – first initiated by the pioneering word of 2007 chemistry Nobel Prize Gerhard Ertl[3] – in turns fashions the opportunity for "catalysis-by-design".[1,4] This is particularly attractive at the nanoscale, where the complexity of the energy landscape of metallic nanoparticles[6] opens challenging but intriguing and rewarding routes in tailoring nanoarchitectures – size, shape, chemical composition, and ordering – to attain high catalytic performances.

Many studies have shown how a substrate can improve the catalytic properties of supported nanoparticles.[7,8] Further, the formation of strong metal-support interactions has been suggested to stabilise nanoparticles' shape also possibly unfavourable in the gas phase.[2] Nonetheless, structural transitions can be significant also in the case of a strong metal-support interaction, as for the case of Pt nanoparticles soft-landed on a pristine MgO(100) surface.[9] Parallel to the presence of several energetically relevant local minima in the potential energy landscape of a nanoparticle, another crucial aspect in the study of nanosized objects thus lies in the analysis of their fluxionality, i.e. the (frequent) occurrence of thermally activated structural rearrangement.[6,10,11] Solid-solid transitions may, in fact, significantly change the nanoparticles' surface[12] and strain distribution[13] and, in turn, lead to a change in the nanoparticles' catalytic performance. The modelling of supported nanoparticles as fuel cell catalysts results in a complex problem, with at least two interfaces to be characterised: (i) the one between the metallic nanoparticle and the support, (ii) the one between the adsorbed molecule(s) and the catalyst.

To our knowledge, in so far there are no numerical approaches that account for thermally activated structural transitions when predicting nanoparticles' catalytic activity. Our novel numerical strategy to this end is based on the sequencing of a nanoparticle genome.[13] With the latter term we refer to the classification and counting of nanoparticle's non equivalent adsorption sites (NEAS), characterised by a suitable geometrical descriptor, e.g. the atop generalised coordination number (GCN).[14] Following the sequencing of the nanoparticle genome we then employ the GCN-based micro-kinetic model recently proposed by Ruck and coworkers[15] to estimate the electrochemical mass activity of Pt-nanoparticles in the gas phase for oxygen reduction reaction. Experiments and theoretical calculations demonstrated a linear scaling relationship between OH* adsorption energy on an adsorption site and the generalised coordination of the latter. Hence, the activity versus site generalised coordination results in a volcano-plot with concave sites resulting the most active.[16] Our assumption is the following: as the OH-chemisorption depends on the local environment of the site at which the molecule binds, the scaling relationship and volcano plot for Pt-nanoparticles in the vacuum is valid in a wide range of temperature and, at least in first approximation, for supported systems too. This hypothesis is especially strong when the adsorption site is relatively far from the substrate.

[a] Dr. K. Rossi, Dr. G. G. Asara, Dr. F. Baletto
Physics Department, King's College London, London WC2R 2LS, UK
E-mail: francesca.baletto@kcl.ac.uk
[b] Dr. K. Rossi
Laboratory of Computational Science and Modeling, Institute des Materiaux, Ecole Polytechnique Federale de Lausanne,
CH-1015 Lausanne, Switzerland

Special Issue An invited contribution to a Special Issue on Electrocatalysis

Beyond the Surface Science approach to thermo- and electro-catalysis, initiated by Ertl on clean surfaces and in well-defined conditions,[4] the inclusion of "ugly" and not-well defined geometries is the new challenge at stake for understanding catalytic processes at the nanoscale.[16] Indeed low-symmetry defected morphologies are likely to be observed during the finite-temperature evolution of a metallic nanocatalyst in operando. Sequencing the nanoparticle genome on the fly during structural re-arrangments opens the intriguing possibility to monitor the evolution of the activity of metallic nanocatalysts at finite temperatures. Here, we thus couple the above micro-kinetic model with classical molecular dynamics to estimate the mass activity of MgO-supported Pt nanoparticles (Pt-NPs) during their dynamical evolution. In turn, we aim to elucidate the degree by which the surface structural rearrangements often occurring during the nanocatalyst lifetime affect nanoparticle's catalytic activity.

In the following study we focus on the structural re-arrangments of Pt-NPs with a size varying from 1.2–2.3 nm when soft landed on a pristine-MgO(100) substrate. Common nanoparticles' geometries such as the icosahedral, decahedral, and cuboctahedral, are taken in account as the initial ones for soft landed nanoparticles. We observe that structural changes mildly affect the activity for sizes below 2 nm. Anyway, NPs with a diameter of 1.2–1.3 nm are found to be not particularly active. The activity of supported Pt-NPs increases around 1.7 nm. At this size decahedral and cuboctahedral geometries present an average mass activity of 0.5 A/mg, which agrees well with available experimental data.[17] Above 2 nm we observe a tendency to increment the nanoparticles' mass activity in correspondence to the first adjustment of the their lowermost layers. Partial differences in mass activity trends are found when contrasting structural evolutions of Ih and Co of 2.1–2.3 nm diameter: the latter result slightly more active than the former. In all the cases under scrutiny the defected morphologies observed just before the formation of a liquid droplet display a better or similar activity with respect to their high-symmetry counterparts. On the other hand, at this stage, the mass activity of a single nanoparticle oscillates significantly, of about 0.2 A/mg, being very sensitive to the fast changes taking place in their GCN-genome.

In the next sections we will discuss the numerical methodology applied to investigate nanoparticle structural rearrangements, the geometrical tools employed to characterise the dynamical evolution of supported Pt-NPs, and the framework used to estimate nanoparticles' catalytic activity. Afterwards, we will present the analysis of the catalytic properties of supported Pt-NPs of different sizes when undergoing thermally activated structural rearrangements. Finally, we will sum up our observations in the conclusion section.

2. Numerical Methodology

We investigate the paradigmatic cases of thermally activated solid-solid transitions occurring after soft-landing Pt-NPs onto a pristine (100) MgO surface and we consider architectures displaying, initially, an icosahedral (Ih), cuboctahedral (Co), or decahedral (Dh) shape. To sample the rearrangements we use a classical Molecular Dynamics code, LoDiS, available on request from www.balettogroup.org, where the freezing/melting process are simulated by concatenated NVT runs. In each, Newton's equations are integrated using a velocity-Verlet with a time step of 5 fs. The temperature of the system is controlled by an Andersen thermostat. Every $\Delta\tau$ steps, the temperature is lowered/increased by a factor ΔT. The ratio $\rho = \Delta T/\Delta\tau$ tunes the cooling/heating rate and in turns affects the kinetics of the solid-liquid and liquid-solid transitions. This procedure allows to get caloric curves, analyse phase changes, and unravel the role of kinetic contributions in melting/freezing caloric curve hysteresis loop.[18]

The interatomic metallic potential, $E_{TBSMA}(r_{ij})$, is derived within the second-moment approximation of the tight-binding formalism,[19]

$$E^i_{TBSMA} = \sum_{j\neq i}^{n_v} A e^{-p\left(\frac{r_{ij}}{r^0}-1\right)} - \sqrt{\sum_{j\neq i}^{n_v} \xi^2 e^{-2q\left(\frac{r_{ij}}{r^0}-1\right)}}; \quad (1)$$

where the sum runs up to the number of atoms n_v within an appropriate cut-off distance around each atom i; r^0 is the bulk nearest neighbour distance; A and ξ are related to the cohesive energy, while p and q and their product tune the stickiness of the potential. Pt-parametrisation against bulk properties yields A = 0.274 eV, ξ = 2.62 eV, p and q equal to 10.71 and 3.84, respectively.

Metal-oxide interaction is modelled implicitly via a double Morse potentials expanded so that the symmetries of the substrate are respected. This approach captures preferential binding while ensuring little computational expenses. Its main downside is that possible thermal dependent corrugation of the substrate are neglected. Following the Vervisch-Mottet-Goniakowski formulation,[20] as adapted in Ref. [9] the metal substrate interaction energy, E_i^{MS} depends on the distance z between the atom and the substrate, weighted by a set of parameters a_i:

$$E_i^{MS}(x,y,z) = a_1(x,y,z)e^{-2a_2(x,y,z)(z-a_3(x,y,z))} - 2e^{a_2(x,y,z)(z-a_3(x,y,z))} \quad (2)$$

where a_i are dependent on the metallic coordination number, CN_i,

$$a_i(x,y,z) = b_{i1}(x,y) + b_{i2}(x,y)e^{-CN_i/b_{i3}(x,y)}, \quad (3)$$

where b_{ij} is a short writing for a set of the c_{ijk} parameters, weighted by trigonometric functions, which ensure that the periodicity and symmetry underlined by the substrate geometry is respected. In the case of a double-square geometry, as for MgO, the trigonometric weighting is

$$b_{ij}(x,y) = c_{1ij} + c_{2ij}\left[cos\left(\frac{2\pi x}{a}\right) + cos\left(\frac{2\pi y}{a}\right)\right] + c_{3ij}\left[cos\left(\frac{2\pi(x+y)}{a}\right) + cos\left(\frac{2\pi(x-y)}{a}\right)\right]. \quad (4)$$

The metallic coordination of each atom i, has been calculated using a Fermi distribution $CN_i = \sum_{j\neq i} \frac{1}{1+e^{m}(r_{ij}/r_c-1)}$, where we choose $m = 5$ and $r_c = 3.468$ Å, corresponding to a 2.5 ofthe Pt atomic radius. The set of 27-parameters c_{ijk} have been fitted versus density-functional calculation to correctly match the adhesion energy of different nanoparticles and Pt-monolayer on MgO.[9] It is reported here in Table 1 for the sake of completeness.

Table 1. Matrix of the c_{ijk} coefficients, taken from Ref. [8] Each subscript i,j,k runs between 1 to 3.

0.289166	0.149843	0.045534
1.545652	0.046514	0.089767
2.742241	−0.261726	−0.004003
1.120724	0.278722	−0.015515
0.027956	0.171355	−0.037242
−0.542610	0.109480	0.046956
1.168890	−0.103545	0.033496
2.282238	0.655619	0.280348
2.093507	−0.230162	0.193065

2.1. Characterisation of Pt-NPs Architectures and Active Sites

To obtain a detailed mapping of the available non-equivalent adsorption sites (NEAS) at the nanoparticle surface we employ the generalised coordination number (GCN). The GCN of a site j is defined as an average coordination number, CN, of the i atoms within a certain cut-off, r_c, from j, and the maximum coordination, CN_{max} of that site,[14]

$$GCN(j) = \sum_{i\in r_{ij}<r_c} \frac{CN(i)}{CN_{max}}. \quad (5)$$

The same formalism can be used to characterise atop, bridge and hollow sites, with CN_{max} depending on the adsorption mode and the crystallographic arrangement of the metallic surface.

For atop site on a FCC metal, the highest coordination, CN_{max}, equals the nominal coordination of an atom in its bulk configuration, namely 12. When the adsorbed molecule sits between two atoms, bridge-site, the maximum coordination for a FCC metal is $CN_{max} = 18$. By the same token, when the molecule adsorbes on a hollow site, i.e. at the centre of a triplet of atoms, the CN_{max} equals 24 for FCC metals.

Recently, the atop GCN has been adopted to estimate current densities and mass activities of electro-catalysts, for oxygen reduction,[15] CO_2 reduction,[22] and CO oxygenation.[23,24] For the case of Oxygen Reduction Reaction, experiments and theoretical calculations demonstrated that the strength of the interaction with OH decreases for increasingly generalised-coordinated sites. In turn the outcome of a coordination-activity analysis displays a characteristic volcano-shape with sites with GCN = 8.33 at its top.[21]

In our previous work,[13] we showed that GCN-based NEAS-sequencing results in a clear determination of size and shape dependent patterns in the evolution of NEAS occurrences. The list of NEAS present in a nanoparticle can be thus thought as a geometrical fingerprint of the nanoparticle itself. Below 1.5 nm of diameter, nanoparticles of any regular shape present a peculiar fingerprint, different from the one of larger nano-architectures presenting the same morphology. Only for diameters of 3.5 nm and above, each nanoparticle morphology presents a characteristic GCN fingerprint which can be considered complete: when increasing the size of the particle no other NEAS presenting novel GCN will appear. Particles with size in between 1.5 and 3.5 instead present a GCN fingerprint close to the one of larger sizes, but incomplete, or whose GCN values are slightly shifted with respect to the ones of larger nano-architectures. NEAS occurrences with respect to size can be predicted from geometric arguments. Within the GCN characterisation framework, adsorption sites at the vertexes of a nanoparticle and in their first neighbourhood are fixed in number. The correspondent signals in the fingerprint appear already at the smallest sizes. Proper edge sites as well as facet sites in their first coordination shell scale linearly with the size of the nanoparticle. Sites at the centre of a facet,'pure-facet' sites, have the same generalised coordination as they would on infinite extended surfaces of the same symmetry and their number scales quadratically with the length of the edge. They appear latest in the fingerprint of close-shell geometries.

The nanoparticle genome – i.e. the collection and enumeration of the NEAS in a nanoparticle – allows to quantitatively infer nanoparticle's catalytic properties in a fast-and-accurate fashion. In the case of oxide supported Pt-NPs, we exclude from the genome calculations atoms within a spherical sector with height of 5 Å and radius equal to the maximum distance from the centre of mass of atomic layer in contact with the substrate – defined as atoms with the z-coordinate above 3 Å for NPs of height above 2 nm (see Figure 1). Such heuristic choice for the spherical sector allows to treat on an equal footing structures presenting both obtuse or acute wetting angles. We would like

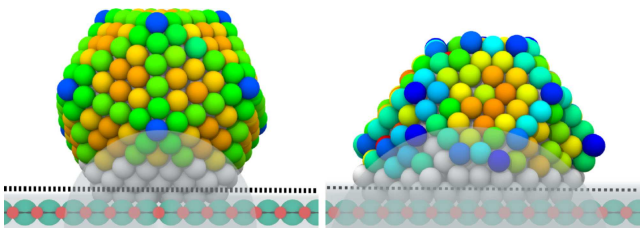

Figure 1. Visual representation of the exclusion zone of active sites (grey) from the calculation of the geometrical genome in the case of supported nanoparticles onto a generic substrate and different wetting properties.

to stress that we aim to estimate the contribution to catalytic performance arising from structural changes induced by the oxide support itself, but any variation of the electronic properties lie outside the paradigm of our assumptions. Due to the distortion induced by the presence of the oxide layer, the cut-off for the first coordination shell is set at 2.5 the atomic radius, against the 2.4 factor used for isolated nanoparticles.[13]

While it is demonstrated that steric hinderance forbids adsorption on surface sites which present a too high generalised coordination,[22] this is not necessarily the case for adsorption sites in contact with the substrate. At least this could depend on the wetting angle formed at the interface. As the scaling relationship employed here refers to isolated nanoparticles and does not include the contribution from the oxide layer, adsorption sites in contact with the substrate are excluded in the calculus of the nanoparticle's genome. In this respect, the reported data represent a lower bound estimate of the nanoparticle's activity. In other words, the *a priori* expectation is that the activity of soft-landed ideal closed-shell nanoparticles is slightly decreased with respect the one of their isolated free-standing counterparts.

2.2. Activity and Coordination

The atop generalised coordination number provides for an accurate classification of adsorption sites while encoding a linear relationship between adsorption site topology and the reaction free energy of OH* intermediates binding on that site. In the model proposed by Ruck et al.,[15] a site with an atop generalised coordination α yields a relative contribution $A(\alpha)$ with respect to the activity form the Pt(111) as:

$$\begin{aligned} A_l(\alpha) &= exp(3.14\alpha - 23.40) \\ A_r(\alpha) &= exp(-4.96\alpha + 42.18) \end{aligned} \tag{6}$$

where A_l and A_r are the left and right end side of the volcano-plot A, respectively. The current produced by a nanoparticle relative to one active site of a Pt(111), $\tilde{j}_{NP}$, is then obtained by summing over all the different NEAS showing a different α.

In their original paper, the authors selected only sites around the top of the volcano-plot, i.e. above 7.5. As the activity contribution from low coordinated sites is much less than the one of highly coordinated, the effect of using different lower-boundaries on the GCN in the calculation of the activity is little. Nonetheless, as the wetting could affect the occurrence of (100) and (111) sites, and at small sizes only few sites are highly coordinated, we opt for including all sites with a GCN above 6. The current density produced by a nanoparticle is found by rescaling the dimensionless $\tilde{j}_{NP}$ with the current density $j_{Pt-flat}$ produced by a (111)-flat surface with a density of sites equal to $1.503 \cdot 10^{15}$ cm^{-2}. Here, we set $j_{Pt-flat}$ to be 2 mA cm^{-2}. The mass activity of a nanoparticle can be then obtained dividing by its mass, which is simply the number of atoms N_{NP} multiplied by the Pt atomic mass. Substituting, the expression of the mass activity in A/mg is

$$MA_{NP} = j_{NP}/M_{NP} = 4.107\,\frac{\tilde{j}_{NP}}{N_{NP}}\,, \tag{7}$$

where $\tilde{j}_{NP}$ is the dimensionless current density relative to the Pt (111) and the pre-factor 4.107 is in A/mg. We support our assumption in using the gas phase scaling relationship for supported nanoparticles, following from the successful use of the atop GCN as a proxy of the adsorption of small molecules on MgO-supported Pt-NPs as discussed in our previous works.[25,26]

3. Results and Discussion

3.1. Activity of MgO-Supported Pt-Nanoparticles During Melting

Under the assumption that the GCN scaling relationship for OH* reduction follows the same scaling relationship as for Pt-NPs in the gas phase we monitor the nanoparticle genome evolution to estimate the activity of supported nanoparticles undergoing structural rearrangements.

As a paradigmatic example, the dynamical evolution of the GCN-genome of two Pt-NPs of 309 atoms soft-landed on MgO during melting is shown in Figure 2. In particular, the case where the initial configuration is an Ih is reported. As we have recently highlighted,[9,11] the transformation of an Ih onto MgO proceeds layer-by-layer toward a FCC-like geometry. This rearrangement happens in a few steps which can be summarised as follows: (i) reconstruction of the first two layers in contact with the oxide-substrate to match the double-square patternof the substrate, (ii) propagation of the reconstruction, layer-by-layer, until the reconstruction into a FCC, (iii) modification of wetting, (iv) formation of a liquid/amorphous shape. The two GCN-genome evolutions reported in Figure 2 highlight how the formation of a few highly coordinated sites at the beginning of the simulation (pink circled region) may occur, these being crucial in determining a high activity for ORR in the system in the right panel.

To investigate the catalytic activity evolution of a nanoparticle with a different initial geometry we consider a Pt-NP soft-landed when presenting a Co-morphology. In Figure 3 we report the dynamical evolution of its GCN-genome. In this case, the only geometrical transition we witness is related to a change in the wetting properties of the nanoparticle. This change is likely to happen within a few ns in the 800–1200 K temperature range, as highlighted by the two pink arrows in Figure 3. During such transition, the nanoparticles looses some of the signals in its GCN-fingerprint but broadens others, especially around the GCN-atop = 6.2–7.2 range, in correspondence of the formation of a few highly coordinated sites.

The activity of Ih and Co Pt-NPs$_{309}$ is compared in Figure 4, where we report per each system the results gathered over four independent runs. At 500 K, during the first 10 ns of sampling, the mass activity of a supported Ih increases significantly up to 0.5 A/mg, in correspondence to the first layer reconstruction.

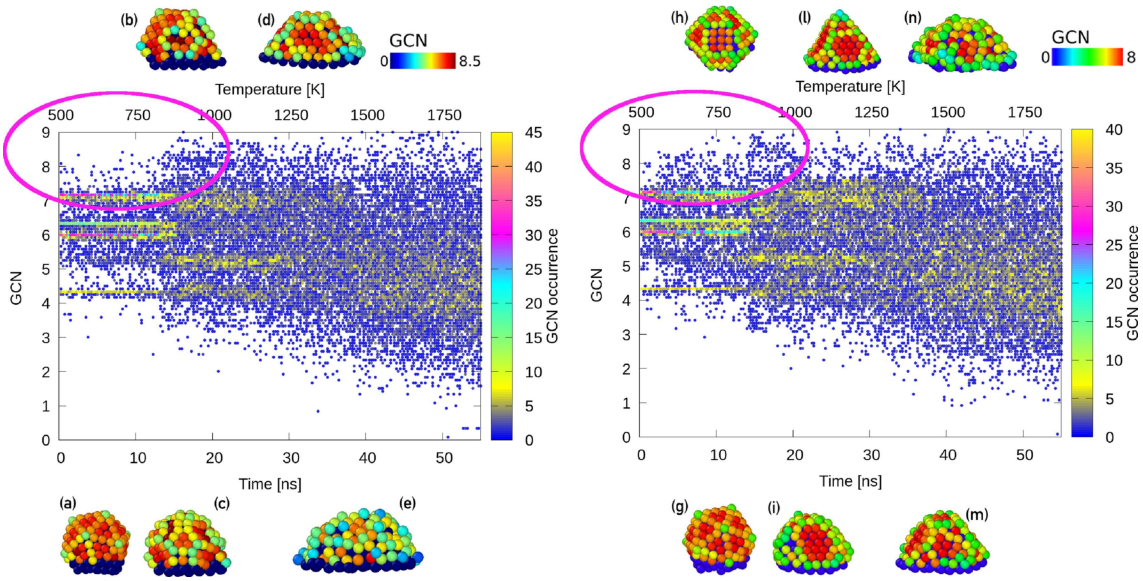

Figure 2. Two independent simulations showing the GCN-genome evolution during the melting of a soft-landed Ih_{309} of Pt onto the pristine MgO. The temperature is risen by 50 K every 2 ns. The colour code in the main panel shows the occurrence of each GCN value. Snapshots are taken at different times, and corresponds to the steps described in the text, highlighting the layer-by-layer transformation of a Ih into a mixed FCC–Ih motif, the change of the wettability, and the phase change. Atoms in the Pt-NP are coloured from blue to dark-red, accordingly to their GCN (low to high). The substrate is not shown for the sake of clarity.

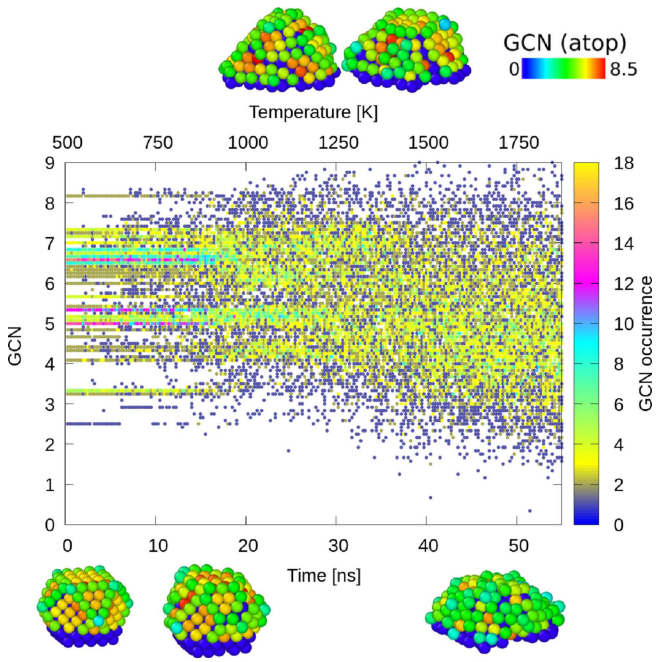

Figure 3. GCN-genome evolution during the melting of a Pt-NPs of 309 atoms displaying initially a Co shape when soft-landed onto a pristine (100) MgO support. To probe the nanoparticle thermal stability the temperature is risen by 50 K every 2 ns. The colour code ollows the one in Figure 2. The change of the wetting lasts between the two pink arrows.

Over this observation conditions, the activity of a Co is instead almost constant around a value of 0.3 A/mg. As structural transitions of Pt-NPs are possibly concerted but likely diffusion-driven, the atomistic details might differ from case to case. This is highlighted in the two examples reported in Figure 2 which corresponds to the activity by red and green lines in the bottom panel of Figure 4, respectively.

The simulation shown in the right panel of 2 (green line) reports the first tens of ns of the simulation to the formation of a few highly coordinated sites and larger (111)-facets which increase the mass activity. This is a common rearrangement, observed in 3 out of 4 simulations. Indeed all but the red curve in the right panel of Figure 4 display an increase in the mass activity. Nonetheless, the first layer rearrangement could also preserve the icosahedral-shell for a longer time-scale ((b) snapshot on the left panel of Figure 2). An increment of the mass activity is then witnessed only in correspondence of the first structural rearrangement into a FCC-shape (snapshot (c) of the same Figure). We further notice that the completion of the reconstruction into a FCC shape, together with changes in in the wetting properties of Pt-NPs, leads to significant oscillations in the mass activity of nanoparticles. These oscillations present a similar intensity to the one observed for melted nanoparticles. An increase of the mass activity is also witnessed when the nanoparticle-wetting changes. This observation is particularly significant for the case of nanoparticle presenting an initial Co. Regardless of the initial nanoparticle shape, a liquid droplet is rapidly formed above 1500 K. It is characterised by a larger contact area with the surface and the presence of only a few layers and a quite disordered surface. Anyway, also this morphology shows an activity similar to its solid-shape counterpart(s). We remark that the estimate of the activity in the 0.3–0.5 A/mg range agrees well with available experimental measurements from Pt/SiO_2 and Pt/C nanocatalysts.[17]

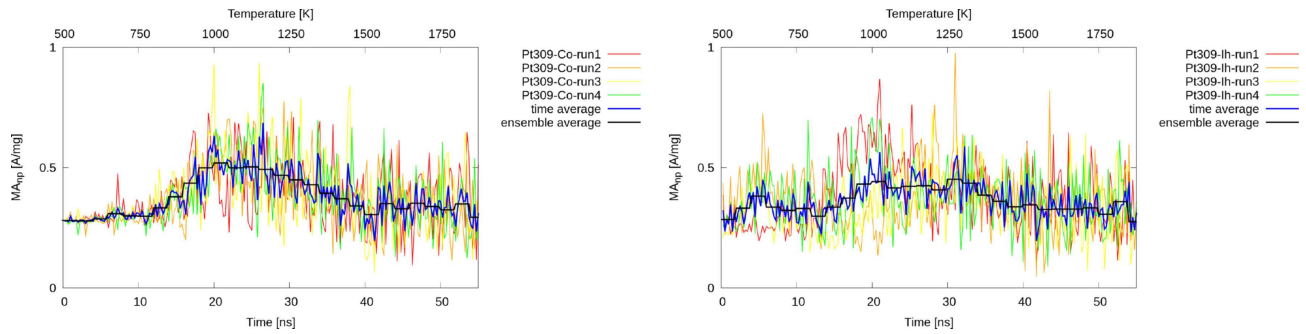

Figure 4. Estimate of the mass activity of MgO-supported Pt-NPs of 2.1–2.3 nm in diameter. Right panelrefers to the melting of an initial Ih while the left one to the melting of a Co. Four independent runs have been performed per each case. Their average per each observation is reported in blue (time average), while the one per each thermodynamic ensemble atfixed temperature is shown in black (ensemble average).

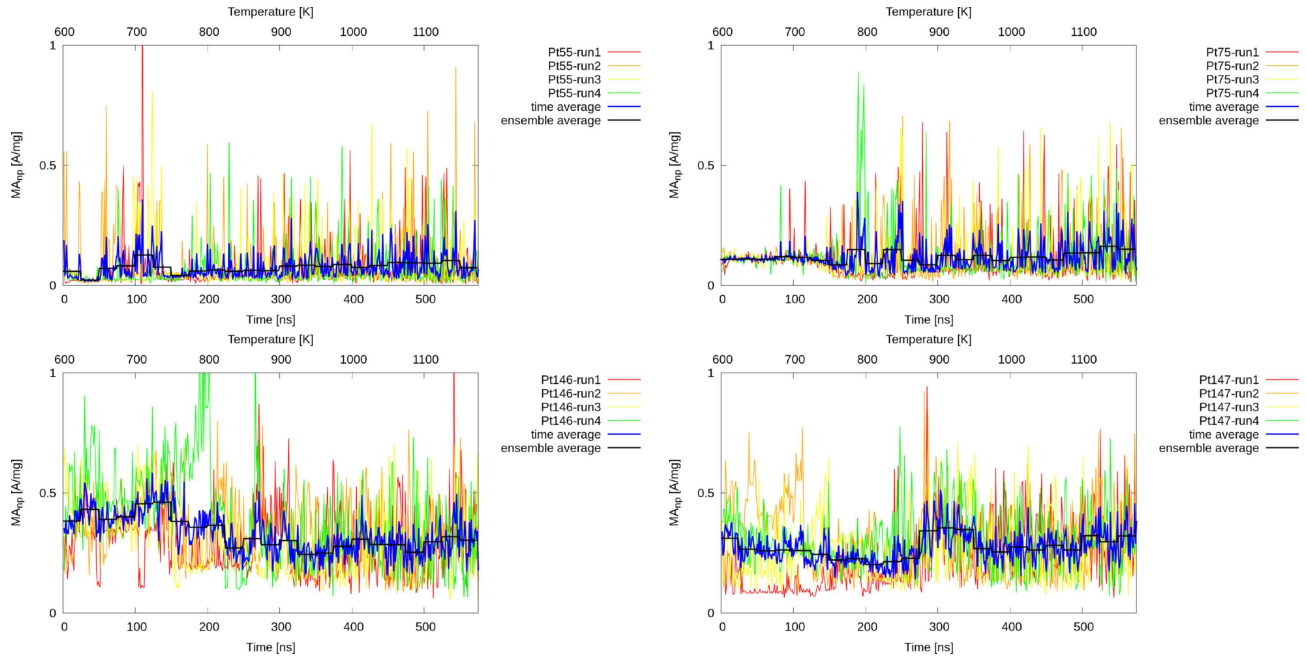

Figure 5. Mass activity of small Pt-NPs as Co_{55} (top-left), Dh_{75} (top-right), Dh_{146} (bottom-left) and Co_{147} (bottom-right). Colours refer to independent simulations. Their average per each observation is reported in blue (time average), while the one per each thermodynamic ensemble at fixed temperature is shown in black (ensemble average). The phase change corresponds to stronger oscillations in the mass activity.

3.2. Activity Versus NP-Size

To address size-effects we also probe the activity of Pt-nanoparticles of sizes 55, 75, 146, 147, and 561 atoms, soft-landed onto a pristine MgO(100) and gradually heated at a rate of 10 K/ns. The activity of Pt-NPs with a diameter smaller than 1.8 nm is shown in Figure 5. As a first notable observation, let us stress the different behaviour of the Dh and Co shapes of 146 and 147 atoms (diameter *d* of 1.7 nm). The former results significantly more active than the latter. Furthermore, depending on which structural transition takes place, we observe some considerable differences in the estimates of each nanoparticles' activity. This highlight that on the fly structural information is key in order to elucidate the properties and improve the design of the next-generation of nanocatalysts. The observed drop in the ORR-activity for Pt-NPs smaller than 1.5 nm agrees well with experimental data.[17] Let us however remark that because of the small size of the nanoparticles under consideration, and the limitations in the micro-kinetic model here employed, the reported data represent a lower-bound estimate on the real activity of such sub-nanometre nanoparticles. We note that their small size is likely to allow for the use of accurate electronic structure methods. In turn, explicit calculations can allow to probe their mass activity with a greater accuracy at a larger but anyway feasible cost.

Some of the features of a Pt_{309} are more evident for a Pt-Ih_{561} soft-landed onto a MgO pristine substrate. This nanoparticle presents an increase in its activity (from 0.4 to 0.5 A/mg) in correspondence of the first structural transition, see Figure 6. Such rearrangement leads to the formation of a mixed

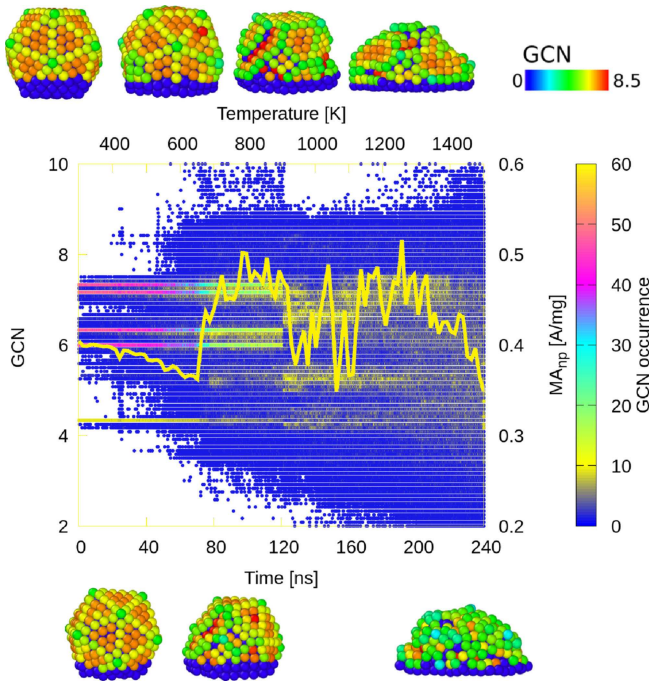

Figure 6. Mass activity of a soft-landed Pt-lh$_{561}$ NPs onto the pristine MgO (the oxide is notreported for sake of clarity). The evolution of the GCN-genome, the activity and few snapshots are reported to stress the interplay between structural changes and activity. The phase change is associated with a decrease of the activity while the mixed shape lh-cup above a few FCC-layers is quite promising. Atoms in various nanoparticles snapshots coloured accordingly to their GCN, from blue sites which are not available for any adsorption, up to red corresponding to a GCN above 8.5.

shape with a few bottom layers in contact with the oxide arranged into a FCC and the upper part still displaying icosahedral features. The sudden drop in the activity is related to the full reconstruction into a FCC-like motif. The activity at high temperature might fluctuate considerably, of around 0.1 A/mg with respect to an average value of 0.42 A/mg. At this observation conditions we assist to several and abrupt changes in the mass activity.

These are due to the frequent appearance of surface defects. Though possibly not definitive, there is some further evidence that approaching the melting phase change might will affect in a negative way the nanoparticle activity in the system under scrutiny.

4. Conclusions

In this manuscript, we have proposed a simple and efficient method to estimate the catalytic activity of MgO-supported platinum nanoparticles by means of classical molecular dynamics. To this end, we monitored the dynamical evolution of the generalised coordination of all the possible adsorption sites of the supported nanoparticles – with the exception of surface sites tooclose from the substrate – and we employ a known scaling relationship for the adsorption energy of OH as a function of the same generalised coordination number to calculate nanoparticle mass activity.

We thus showed how structural changes could have a significant impact on estimating the activity of supported Pt-NPs from 1 to a few nm in diameter. Structural reconstructions occurring at the oxide-interface improve the activity, especially when leading to a mixed shape with features reminiscent of FCC and Ih. Strain induced by different wetting properties and structural rearrangements at the interface, even if not altering completely the nanoparticle shape, affect considerably the nanoparticle activity. Further, the formation of liquid-like shapes (phase changes during a melting for example) lead to strong oscillations of nanoparticle catalytic activities and, eventually, to a decrease in its activity.

This observation is particularly relevant for the case of nanoparticles larger than few nm.

Our findings highlight the crucial role structural transitions could play in determining the activity of nanocatalysts. In turn our observations pinpoint the need to characterise and harness the interface between support and metallic nanoparticles to predict and tailor the activity of realistic nanocatalysts.

Acknowledgements

GGA and FB thank the Towards an Understanding of Catalysis on Nanoalloys (TOUCAN) EPSRC Critical Mass Grant (No. EP/J010812/1) as does KR (Grant Reference ER/M506357/1). GGA is grateful to the postdoctoral scheme offered by the NMS faculty. All the authors are grateful to the financial support offered by the Royal Society (No. RG 120207) via our membership of the UK's HEC Materials Chemistry Consortium, which is funded by the EPSRC (EP/L000202). This work used the UK Materials and Molecular Modelling Hub for computational resources, MMM Hub, which is partially funded by the EPSRC (EP/P020194).

Conflict of Interest

The authors declare no conflict of interest.

Keywords: electrocatalysis · generalised coordination number · molecular dynamics · platinum · supported nanoparticle

[1] C. R. Catlow, M. Davidson, C. Hardacre, G. J. Hutchings, *Phil. Trans. Royal Soc. London A* **2016**, *374*, 2061.
[2] S. Sui, X. Wang, X. Zhou, Y. Su, S. Riffat, C. J. Liu, *J. Mater. Chem. A* **2017**, *5*, 1808.
[3] G. Ertl, **2007**, https://www.nobelprize.org/nobel_prizes/chemistry/laureates/2007/ertl-lecture.html.
[4] P. Strasser, M. Gliech, S. Kuehl, T. Moeller, *Chem. Soc. Rev.* **2018**, *47*, 715.
[5] J. Aarons, L. Jones, A. Varmbhia, K. E. MacArthur, D. Ozkaya, M. Sarwar, C. Skylaris, P. D. Nellist, *Nano Lett.* **2017**, *17*, 4003–4012.
[6] D. Schebarchov, F. Baletto, D. J. Wales, *Nanoscale* **2018**,10,2004–2016.
[7] H. J. Freund, G. Pacchioni, *Chem. Soc. Rev.* **2008**, *37*, 2224–2242.
[8] H. Kuhlenbeck, S. Shaikhutdinov, H. J. Freund, *Chem. Rev.* **2013**, *113*, 3986–4034.
[9] K. Rossi, T. Ellaby, L. O. Paz-Borbon, I. Atanasov, L. Pavan, F. Baletto, *J. Phys.: Cond. Mat.* **2017**, *29*, 145402.

[10] L. Pavan, K. Rossi, F. Baletto, *J. Chem. Phys.* **2015**, *143*, 184304.
[11] F. Baletto, *J. Phys. Condens. Matter* **2019**, *31*, 113001.
[12] M. Mavrikakis, B. Hammer, J. K. Nørskov, *Phys. Rev. Lett.* **1998**, *81*, 2819.
[13] K. Rossi, G. G. Asara, F. Baletto, *Phys. Chem. Chem. Phys.* **2019**, *21*, 4888–4898.
[14] F. Calle-Vallejo, J. I. Martinez, J. M. Garcia-Lastra, P. Sautet, D. Loffreda, *Angew. Chem. Int. Ed.* **2014**, *53*, 8316–8319; *Angew. Chem.* **2014**, *126*, 8456–8459.
[15] M. Ruck, A. Bandarenka, F. Calle-Vallejo, A. Gagliardi, *J. Phys. Chem. Lett.* **2018**, *9*, 4463–4468.
[16] F. Calle-Vallejo, J. Tymoczko, V. Colic, Q. Vu, D. Pohl, K. Morgenstern, D. Loffreda, P. Sautet, W. Schuhmann, A. Bandarenka, *Science* **2015**, *350*, 185–189.
[17] F. J. Perez-Alonso, D. N. McCarty, A. Niersoff, P. Hernandez-Fernandez, C. Strebel, I. E. L. Stephens, I. J. H. Nielsen, I. Chorkendorff, *Angew. Chem. Int. Ed.* **2012**, *51*, 4641–4643; *Angew. Chem.* **2012**, *124*, 4719–4721.
[18] K. Rossi, L. B. Partay, G. Csanyi, F. Baletto, *Sci. Rep.* **2018**, *8*, 9150.
[19] V. Rosato, M. Guillope, B. Legrand, *Phil. Mag. A* **1989**, *59*, 321–336.
[20] W. Vervisch, C. Mottet, J. Goniakowski, *Phy. Rev. B* **2002**, *65*, 2454111–2454119.
[21] F. Calle-Vallejo, M. D. Pohl, D. Reinisch, D. Loffreda, P. Sautet, A. S. Bandarenka, *Chem. Sci.* **2017**, *8*, 2283–2289.
[22] M. D. Pohl, S. Watzele, F. Calle-Vallejo, A. S. Bandarenka, *ACS Omega* **2017**, *2*, 8141–8147.
[23] M. Jorgensen, H. Grönbeck, *ACS Catal.* **2017**, *7*, 5054–5061.
[24] H. Xu, D. Cheng, Y. Gao, X. C. Zeng, *ACS Catal.* **2018**, *8*, 9702–9710.
[25] G. G. Asara, L. O. Paz-borbon, F. Baletto, *ACS Catal.* **2016**, *6*, 4388–4393.
[26] O. L. Paz-Borbon, F. Baletto, *Inorganics* **2017**, *5*, 43.

Manuscript received: June 5, 2019
Revised manuscript received: July 26, 2019
Accepted manuscript online: August 6, 2019
Version of record online: September 3, 2019